Eur. Phys. J. C 49, 767–782 (2007)
DOI 10.1140/epjc/s10052-006-0131-4

THE EUROPEAN PHYSICAL JOURNAL C

Regular Article – Theoretical Physics

Parton bubble model for two-particle angular correlations at RHIC/LHC

S.J. Lindenbaum[1,2,a], R.S. Longacre[1]

[1] Brookhaven National Laboratory, Upton, NY 11973, USA
[2] City College of New York, New York, NY 10031, USA

Received: 19 May 2006 / Revised version: 7 September 2006 /
Published online: 15 November 2006 –

Abstract. In an earlier publication we developed a bubble model, based on our evolution of the original ideas of van Hove which we concurred with over two decades ago; namely, that if a quark–gluon plasma is produced in a high energy heavy ion collider, then some of its hadronization products could be emitted from small bubbles localized in phase space containing plasma. In this paper we refined the model to become a parton bubble model in which each localized bubble contains initially 3–4 partons which are almost entirely gluons forming a gluon hot spot. We greatly expanded the transverse momentum interval investigated and thus are able to treat recombination effects within each bubble. We again utilize two-particle correlations as a sensitive method for detecting the average bubble substructure. In this manuscript we make many predictions for angular correlations detectable at RHIC, which will be later modified to LHC conditions. A quantitative test of the multi-bubble substructure assumed in the model was made by comparing with precision STAR Collaboration correlation analyses. Good quantitative agreement was obtained. Some early available low precision correlation analyses is qualitatively explained.

1 Introduction and general considerations

In an earlier publication [1] we introduced a bubble model. In this paper we further developed our evolution of the original ideas of van Hove with which we concurred with over two decades ago [2–7]; namely, that in heavy ion collisions at energies that are accessible at colliders such as RHIC or LHC, if a quark–gluon plasma (QGP) is created, it might produce bubbles (or droplets) containing QGP localized in phase space. In [1] we proposed a bubble model for high energy heavy ion collisions, consisting of a single ring of 13 adjoining 2 fm radius bubbles transverse to the collider beam direction, centered on the beam, and located at or near mid-rapidity. Figure 1 of this paper has 12 bubbles in the ring and represents the bubble geometry used in this paper. Reference [1] had 13 bubbles in the ring because that was the mean number of that prior calculation. Thus though the two figures are very similar they are not identical. Therefore Fig. 1 is the geometry for the final state kinetic freeze-out of the QGP bubbles on the surface of the expanding fireball. In the central (near impact parameter 0) mid-rapidity region at RHIC we are observing the region where the highest energy densities and temperatures (parton energies) are produced. The $\sqrt{s_{NN}} = 200$ GeV central Au + Au collisions at RHIC produce initial energy densities [8] which exceed those predicted by lattice quantum chromodynamics (QCD) as sufficient for production of a QGP [9].

In this paper we are concerned with making model predictions which can, by comparing with experimental analyses, test whether a localized bubble (gluonic hot spots) substructure exists. After a successful demonstration of this, we plan in a later stage to search for QGP characteristics arising from the bubbles. Evidence for a bubble substructure (dense gluonic hot spots) perhaps originating from a quark–gluon plasma (QGP) could be found in particle correlations produced in these collisions.

1.1 Motivation for the model

Our motivation for the evolution of the bubble model has been the following: In the early eighties it was reasonable to expect that high gluon densities would be produced at RHIC in central Au + Au collisions at $\sqrt{s_{NN}} = 200$ GeV/c. Due to strong attraction between gluons of low relative momenta one could speculate that clusters or bubbles of higher density gluons (gluonic hot spots) localized in phase space would form. The van Hove model [2] proposed in 1984–1985 was a good illustration of this possibility. The actual dynamics of formation of these clusters or bubbles and their evolution to the final state at freeze-out involved strong non-perturbative QCD effects and dynamical effects. These effects are enormously complex and are not understood, because they involve

[a] e-mail: lindenbaum@bnl.gov

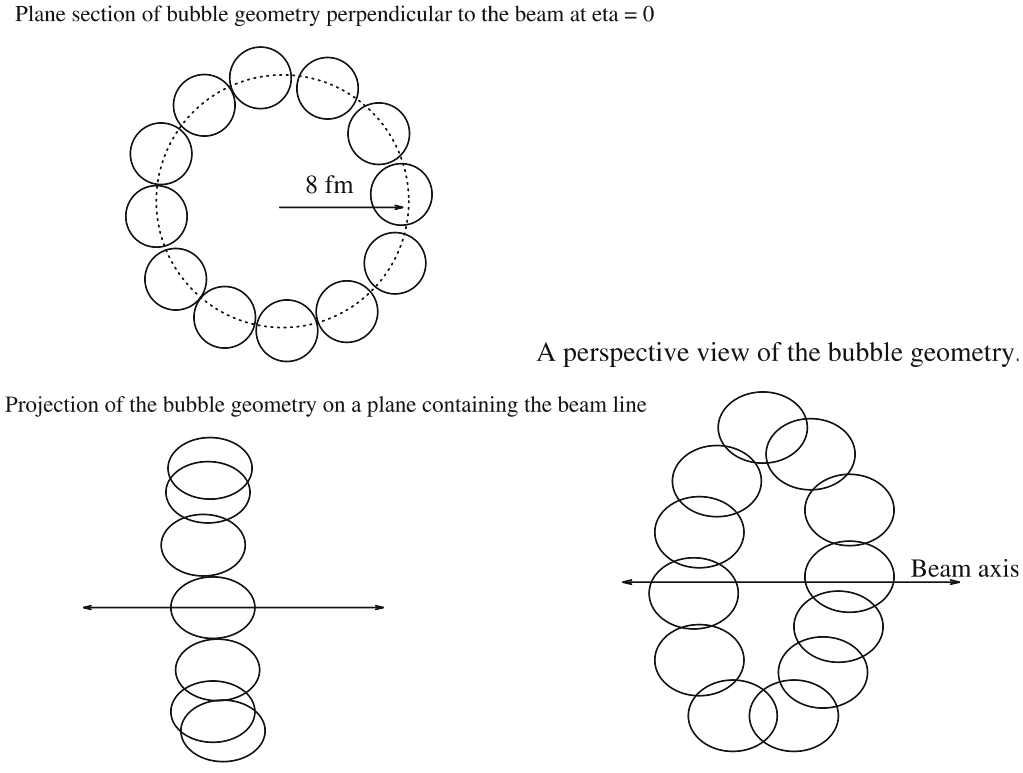

Fig. 1. The bubble geometry is an 8 fm radius ring perpendicular to and centered on the beam axis. It is composed of twelve adjacent 2 fm radius spherical bubbles elongated along the beam direction by the Landau longitudinal expansion. The *upper left figure* is a projection on a plane section perpendicular to the beam axis. The *lower left figure* is a projection of the bubble geometry on a plane containing the beam axis. The *lower right figure* is a perspective view of the bubble geometry. Due to rotational invariance about the beam axis the only direction that is meaningful to define is the beam axis shown in the *lower two figures*

a series of processes, many of which are not known and calculable. Thus they could at best only be approximated by models such as a string model or other models. Therefore one could only speculate, and hope that future experimental observations would possibly provide evidence for such substructures. With the observation of substructures, they become input to theoretical models. Such a model could then be tested by comparison with experimental data analyses sensitive to such substructures. Depending on the uniqueness of the substructure signals, convincing evidence for these bubbles might be established.

Whether a QGP is formed or not formed, the evidence for substructure and a way to isolate these substructures makes it possible to do further detailed analyses. If QGP signatures exist in these substructures (bubbles) then one could have an enriched sample that could eventually provide evidence for the QGP.

Observations using the Hanbury–Brown and Twiss quantum interference (HBT) [10, 11] show that the final state source size has a dimension characterized by a radius of 6 fm at low p_t. This source size reduces with increasing p_t to approximately 2 fm at or above a p_t value of 0.8 GeV/c. We used the above fact to postulate a bubble substructure in the final state with the radial dimension of each bubble approximately 2 fm. This led to [1] and the present parton bubble model presented in this manuscript. Reference [1] also led to the STAR experimental data analyses [12] which were designed to provide a quantitative test for the model [1]. The parton bubble model presented in this manuscript is a parton inspired version of [1]. In Sect. 4 we compare the STAR experimental analysis [12] with our analysis of parton bubble model generated events and find good quantitative agreement.

A letter [13] quoted and discussed in [1] was relevant to our work since it predicted a range of domain sizes (bubbles or gluonic hot spots) one of which was 2 fm which coincided with our HBT based estimate. Two earlier papers [14, 15] considered gluonic hot spots and are of interest, but they were not used in our work.

In summary our original motivation was the van Hove model, which was the earliest, and predicted how to check it quantitatively by experiments. Our manuscript in 2000 [7] predicted striking signals for isolated bubbles (gluonic hots spots) which were not observed. The HBT work and our interpretation of it as due to a multi-bubble substructure of radial dimensions approximately 2 fm is described in [1] and the present manuscript. These ideas allowed us to build a model based on striking experimental observations.

1.2 General details

The bubble ring radius of our model was estimated by blast wave and other general considerations to be approximately 8 fm [1]. This single bubble ring resides on the surface of the expanding fireball at freeze-out. Each bubble might emit a considerable fraction of final state particles resulting from the QGP state, and there would be very little re-interaction for those emitted outward from the surface because the surface of the fireball is at freeze-out. The choice of the 2 fm radius was motivated by the HBT [10, 11] observations which have shown that at low p_t the final state

source size radius is about 6 fm, whereas above 0.8 GeV/c the source size reduced to about a 2 fm radius.

The 2 fm source size observed by HBT analyses was interpreted as phase space focusing of the viewed region of the overall source becoming smaller and near the surface as one selects particles with p_t values higher than 0.8 GeV/c. Phase space focusing makes it possible for these higher p_t particles to view and resolve individual 2 fm radius regions (bubbles) on the surface of the expanding fireball. If there is such a bubble substructure it would appear as angular regions of greater particle production above a p_t momentum of 0.8 GeV/c. Therefore two-particle angular correlations could detect this bubble substructure. The difference in angle particle correlation techniques we are employing are powerful methods in determining bubble substructure since it is the relative angles of the two particles, not their position on the fireball surface, that is important. Thus our bubble ring of approximately 2 fm radius bubbles would lead to the phase space focusing which produced the approximately 2 fm final state source size observed by HBT [10, 11], since the 12 bubbles would image on top of each other.

In [1] we took account of the well known Landau longitudinal expansion of the fireball that causes the angular spread of particles to be much larger in the longitudinal direction than the transverse. This longitudinal expansion of the fireball will continue to be an important feature of the present manuscript.

In this paper we expand the model of [1] and employ a 12 bubble ring similar to the previous work (which had 13 bubbles), but treat mid-rapidity Au + Au $\sqrt{s_{NN}} =$ 200 GeV central production (impact parameter near 0). Using some RHIC Au + Au data with $\sqrt{s_{NN}} = 200$ GeV, we adjusted our model and make predictions for angular correlation analyses of charged particles emitted from the surface of the fireball.

We will concentrate on the experimentally observed particle pair angular correlations in the transverse momentum region 0.8 GeV/$c < p_t <$ 4.0 GeV/c, except those at small relative angles where Coulomb and HBT effects occur. Background resonances are also considered unimportant. Figure 1 shows a sketch of the bubble geometry used. Our goal is to develop a parton inspired bubble model. Thus we assume that essentially all mid-rapidity two-particle angular correlations in the final state of central heavy ion collisions, except the small angle Coulomb and HBT effects, results from particle emission by the parton bubbles formed on the outer surface of the expanding fireball. The present paper will concern itself with predictions that are testable at RHIC. However, when sufficient knowledge of the characteristics of future LHC data becomes available we intend to apply these ideas, suitably modified for conditions at LHC, to those data. We speculate that at the much higher LHC energies there will be localized gluonic hot spots (bubbles) on the surface of the fireball at freeze-out, and the resultant particle emission from the bubbles is the dominant factor determining the experimentally observed correlation structure. It is possible that unforeseen phenomena could drastically change the correlation structure. Excluding this possibility, we need to know two major factors in order to apply the parton bubble model. The first is the HBT analyses as a function of p_t which will give the approximate radial bubble dimension. The second is a blast wave fit of the LHC data to determine the overall size of the freeze-out surface and the p_t range of the surface bubbles. These two factors will define the bubble ring geometry and its characteristic parameters corresponding to those cited in Table 1. The p_t (GeV/c) and energy (GeV) in Table 1 would likely both increase as the energy of colliding heavy ions increases.

Table 1. Parameters of bubble model for charged particles

Variable	Amount	Fluctuations	Systematics
Bubbles	12	0	0
Particles	7.3	2	0.7
Soft	104	12	0
p_t (GeV/c)	6.0	0.8	0.3
Energy (GeV)	9.0	4.0	2.0

In our earlier work [1], we made a cut on the transverse momentum 0.8 GeV/$c < p_t <$ 2.0 GeV/c. The lower bound was chosen to resolve individual bubbles and take advantage of phase space focusing to enhance the bubble signal, by adding up contributions from many bubbles. The upper bound was chosen in order to avoid possible jet fragmentation contamination. However, now it is clear that jets are strongly quenched [16, 17], and provided one does not use a jet trigger the particles in the 2.0 to 4.0 GeV/c p_t range are not the usually expected jet fragmentation particles. For example many of the particles exhibit η elongation very inconsistent with jet characteristics [18]. In the present work we think it is reasonable to assume that a large fraction of the particle correlations in the 0.8 to 4.0 GeV/c p_t range come from bubbles. Expanding our upper cut to 4.0 GeV/c allows us to explore quark–quark recombination [19] and various combinations of two-particle correlations such as for example angular correlations of protons and antiprotons with other charged particles. The kinematical consequences of quark–quark recombination require the consideration of this higher p_t cutoff. Furthermore it appears reasonable to make the approximation that for central Au + Au collisions at RHIC, jet fragmentations from parton–parton scattering are small compared to our bubble fragmentation, because of jet quenching. Parton–parton scattering is an initial state effect which is reduced by the medium, whereas our bubbles are the final state source on the outer surface of the fireball.

2 Our parton bubble model

In our earlier work [1], we constructed a model for bubble formation based on the modification of the HIJING event generator [20]. The most important modification was the replacement of the jets (sometimes referred to as mini-jets) with bubbles. We also modified the particles from the remaining beam jets fragmentation by including the effects of elliptic flow. For this work HIJING is further modified

so as to merely become a source of background particles. HIJING has two relevant sources of particle production: jets which fragment into particles which are referred to as jet particles, and the soft particles which come from beam jet fragmentation. The jet particles are not flat in azimuth but bunch around the jet axis. The beam jets fragmentations are very flat in azimuth.

Also in this work we make the approximation that jet particles are essentially removed or have their correlations eliminated by quenching, and thus there are no correlations left due to jets. Only the soft beam jet particles from HIJING are left, and they do not have any correlations. Therefore, they are our background particles in the correlation investigations. However, we did include the effects of elliptic flow [21–23] on the soft beam jet particles since elliptic flow does generate a small $\cos(2\Delta\Phi)$ term in the correlation. Momentum, energy, and charge conservation are all satisfied within the bubble ring in this model.

2.1 The correlation function

We utilize a two-particle correlation function in the two dimensional (2D) space of $\Delta\Phi$ versus $\Delta\eta$. The azimuthal angle Φ of a particle is defined by the angle of the particle with respect to the vertical axis which is perpendicular to the beam axis and is measured in a clock-wise direction about the beam. $\Delta\Phi$ is the difference, $\Phi_1 - \Phi_2$, of the Φ angle of a pair of particles (1 and 2). The pseudo-rapidity η of a particle is measured along one of the beam directions. $\Delta\eta$ is the difference, $\eta_1 - \eta_2$, of the η values of a pair of particles (1 and 2).

The 2D total correlation function is defined by

$$C(\Delta\Phi, \Delta\eta) = S(\Delta\Phi, \Delta\eta)/M(\Delta\Phi, \Delta\eta)\,, \qquad (1)$$

where $S(\Delta\Phi, \Delta\eta)$ is the number of pairs at the corresponding values of $\Delta\Phi, \Delta\eta$ coming from the same event, after we have summed over all the events. $M(\Delta\Phi, \Delta\eta)$ is the number of pairs at the corresponding values of $\Delta\Phi, \Delta\eta$ coming from the mixed events, after we have summed over all our created mixed events. A mixed event pair has each of the two particles chosen from a different event. We make on the order of 10 times the number of mixed events as real events. We rescale the number of pairs in the mixed events to be equal to the number of pairs in the real events. This procedure implies a binning in order to deal with finite statistics. To enhance comparison we use the same binning in our simulations as is used by the STAR high precision experimental analyses [12]. The division by $M(\Delta\Phi, \Delta\eta)$ for the experimental data essentially removes or drastically reduces acceptance and instrumental effects. If the mixed pair distribution was the same as the real pair distribution $C(\Delta\Phi, \Delta\eta)$ would be 1 for all values of the binned $\Delta\Phi, \Delta\eta$. This difference correlation function has the defined property that it only depends on the differences of the azimuthal angle ($\Delta\Phi$) and the beam angle ($\Delta\eta$) for the two-particle pair. Thus the two dimensional difference correlation distribution for each bubble which is part of $C(\Delta\Phi, \Delta\eta)$ is similar for each of our 12 bubbles and will image on top of each other.

In experiments one often separates the total correlation into signal and background correlations. Therefore the total correlation = signal correlation + background correlation.

When we refer to a correlation in this paper without a qualifier, it equals the total correlation, which is sometimes explicitly stated for clarity. If it is the signal correlation, the qualifier signal is added. If it is background correlation, the qualifier background is added.

2.2 Details of the model

A parton that forms a jet fragments into particles through a QCD shower process which finally forms quarks and antiquarks in colored pairs. These quarks and antiquarks combine into color singlet hadrons which form the jet particles. The spectrum of initial jet partons is given by the saturation scale and perturbative quantum chromodynamics (pQCD) cross sections. The parton scattering occurs as binary scattering of two partons leading to a dijet structure. The dijets to lowest order scatter in opposite azimuthal directions (back to back), while the amount of longitudinal momentum varies. Each jet has a well defined η and Φ direction (see Fig. 2).

Particle production from our bubbles uses a similar parton QCD shower fragmentation as a jet with a well defined Φ angle. Inside the bubble there are 3–4 partons with differing longitudinal momentum (see Fig. 3). The p_t distribution of the partons inside the bubble is similar to pQCD but has a suppression in the high p_t region like the

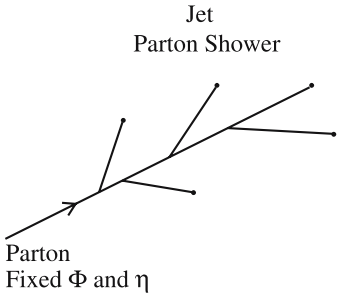

Fig. 2. A jet parton shower

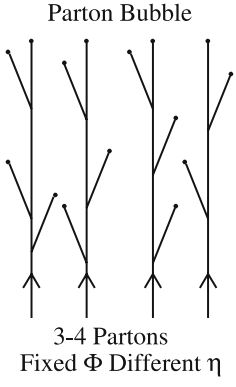

Fig. 3. Each bubble contains 3–4 partons as shown

data [16, 17]. We use Pythia fragmentation functions [24] for the bubble fragmentation.

Due to complexity and lack of knowledge of this complex process which involves non-perturbative QCD, and collision dynamical effects, it is not practical to calculate the number of partons in a bubble or the longitudinal momentum of each parton. Therefore we utilized comparison of some similar STAR data to adjust these. The parton bubble model simulations used the transverse momentum range $0.8 < p_t < 2.0\,\mathrm{GeV}/c$ in order to match the experimental data; see Figs. 4 and 5, which illustrate how good an agreement we obtain between the STAR data and the model after these adjustments.

The STAR experiment has measured charged particle pair correlations for approximately 0–10% centrality Au + Au events at $\sqrt{s_{NN}} = 200\,\mathrm{GeV}$ [25]. The p_t range of that data is 0.8 to $2.0\,\mathrm{GeV}/c$ for the η range $|\eta| < 1.0$. Two $\Delta\eta$ bins are presented in that analysis ($0.0 < \Delta\eta < 0.3$ and $0.6 < \Delta\eta < 0.9$). The adjustable parameters in our parton bubble model are the number of partons per bubble and their longitudinal distribution. 200 000 model events were generated to compare with the STAR analysis. These events had the same p_t range as the data. For each simulated event we added the particles emitted from 12 bubbles and enough soft beam jets in order to have an average of 186 charged particles per event in order to agree with the data. We adjusted the model simulated data to the STAR data to determine the number of partons per bubble and their longitudinal momenta.

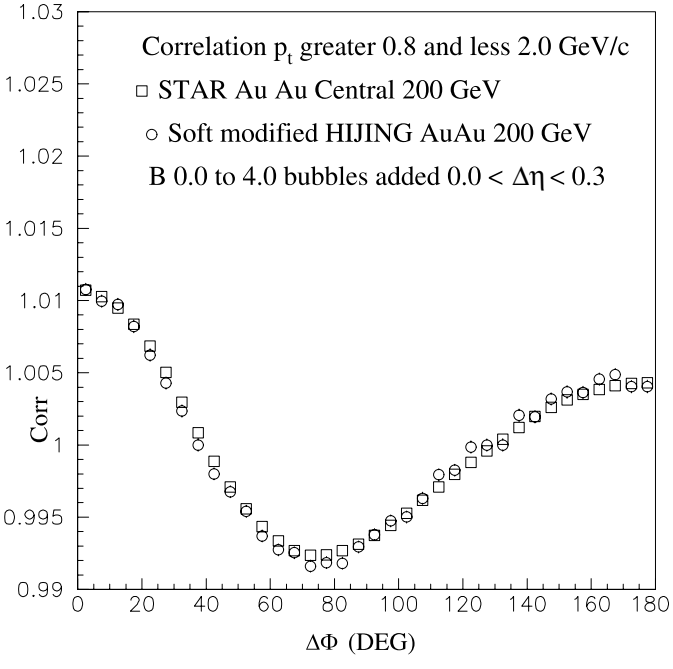

Fig. 4. The $\Delta\Phi$ charged particle pair correlation for soft modified HIJING plus bubbles, which is the bubble model, compared to [25] data for $\Delta\eta$ ($0.0 < \Delta\eta < 0.3$). The 0 –10% centrality in HIJING corresponds to impact parameter (b) range 0.0 to 4.0 fm. The agreement is very good

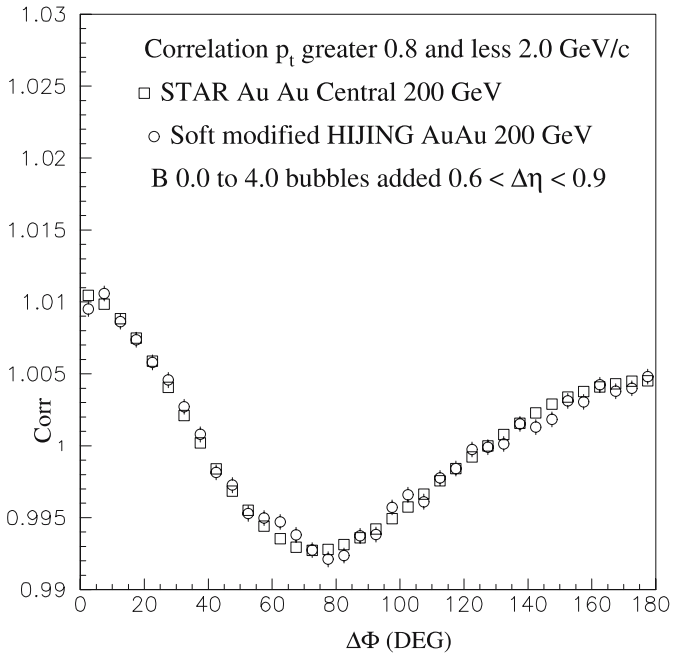

Fig. 5. The $\Delta\Phi$ charged particle pair correlation for soft modified HIJING plus bubbles, which is the bubble model, compared to [25] data for $\Delta\eta$ ($0.6 < \Delta\eta < 0.9$). The 0–10% centrality in HIJING corresponds to impact parameter (b) range 0.0 to 4.0 fm. The agreement is very good

Figure 4 shows the particle pair correlation for soft modified HIJING plus bubbles, which is the bubble model, compared to [25] data for the $\Delta\eta$ bin ($0.0 < \Delta\eta < 0.3$). The 0–10% centrality region in HIJING corresponds to an impact parameter (b) range of 0.0 to 4.0 fm. The away side (beyond 90°) bump in Fig. 4 is due to momentum conservation in the ring of bubbles plus a reaction plane generated elliptic flow v_2 consistent with RHIC data (mean v_2 equals 0.035) [12, 21–23]. Figure 5 shows the model for the $\Delta\eta$ bin ($0.6 < \Delta\eta < 0.9$) compared to [25]. The agreement between the bubble model and the RHIC data in Figs. 4 and 5 is very good.

3 Parton bubble model correlation predictions

Let us look at some correlation predictions of the bubble model we have adjusted to the STAR data. First we plot the part of the correlation that comes from a single bubble considering unlike-sign charged track pairs, for $|\eta| < 1.0$ and p_t from 0.8 to $4.0\,\mathrm{GeV}/c$. Figure 6 is a 2D perspective plot of $\Delta\Phi$ versus $\Delta\eta$ for the part of the unlike-sign charged pair correlation signal which has contributions from particles coming from the same bubble. All other combinations of pairs are subtracted. The particles emitted from a bubble are all signal particles which contribute to correlations.

The particles emitted from one bubble are uncorrelated to particles emitted from another bubble, except for momentum conservation requirements. The particles

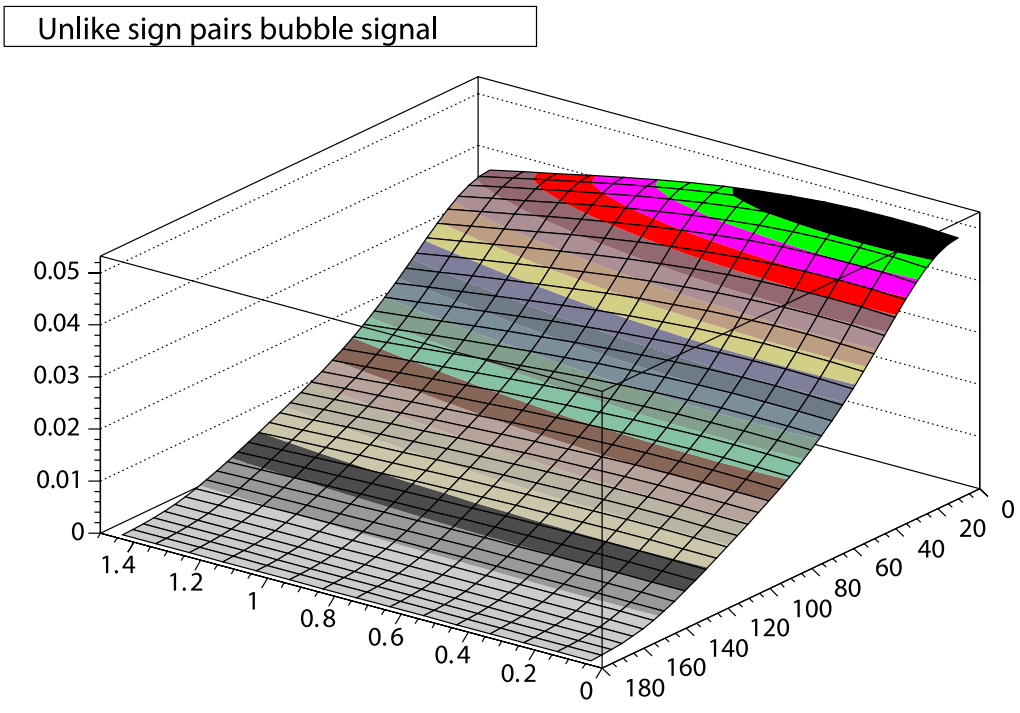

Fig. 6. A 2D perspective plot of $\Delta\Phi$ (*right side scale*) versus $\Delta\eta$ (*left hand scale*) for the part of the unlike sign charged pair correlation signal which has contributions from particles coming from the same bubble. All other combinations of pairs are subtracted. In Figs. 6–9, because of subtraction, 0 corresponds to 0 correlation

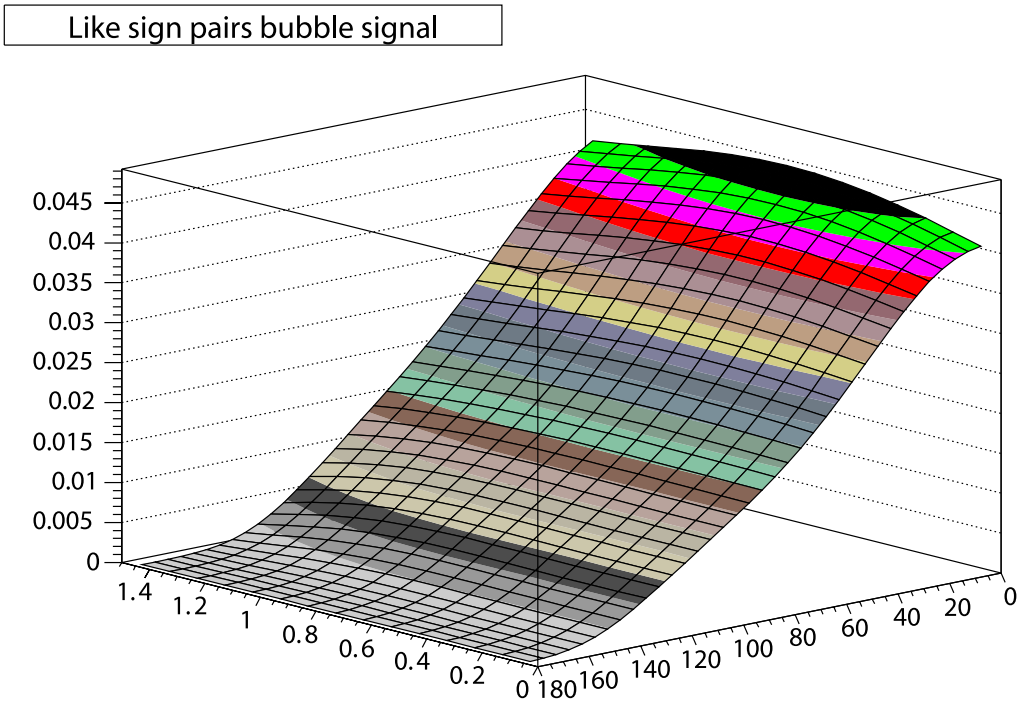

Fig. 7. A 2D perspective plot of $\Delta\Phi$ (*right side scale*) versus $\Delta\eta$ (*left hand scale*) for the part of the like sign charged pair correlation signal which has contributions from particles coming from the same bubble. All other combinations of pairs are subtracted

from the HIJING beam jet particles are background particles and do not contribute to the correlation except for a small amount of elliptic flow. The total correlation of the bubble model is the sum of the correlation of all the pairs. The away side peak (beyond 90°) in the total correlation of the parton bubble model is built up from momentum conservation between the bubbles and is an important contribution to the total correlation predicted by the model and not a background. Therefore in comparing the model with experiment one should compare the total correlation.

In Fig. 6 the $\Delta\Phi$ range is 0° to 180° and the $\Delta\eta$ range is 0.0 to 1.5. We see that the total width in the $\Delta\Phi$ direction is about 60°. The $\Delta\eta$ width is very large, dropping from a high of 0.047 to 0.034 in the $\Delta\eta$ range of 0.0 to 1.5. If this was a Gaussian in $\Delta\eta$, the width would be 1.86,

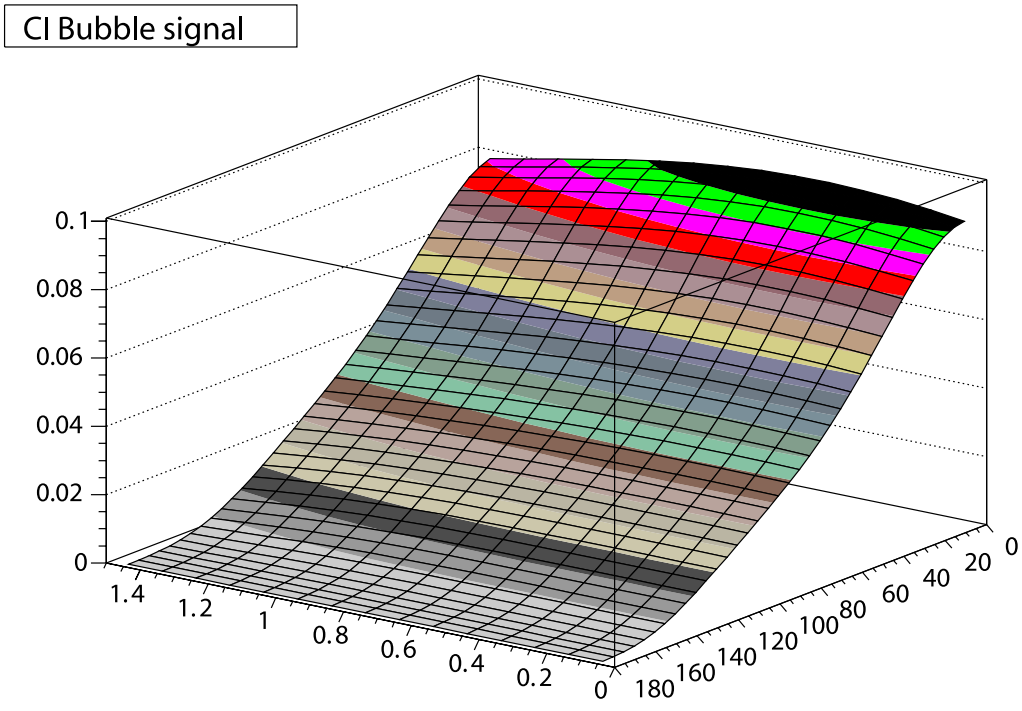

Fig. 8. A 2D perspective plot of $\Delta\Phi$ (*right side scale*) versus $\Delta\eta$ (*left hand scale*) for the charge independent correlation (CI) signal for track pairs from the same bubble. All other combinations of pairs are subtracted. This figure displays the average correlation of particles coming from individual bubbles. The emission of particles from the bubble is by pair production from partons which are almost entirely gluons

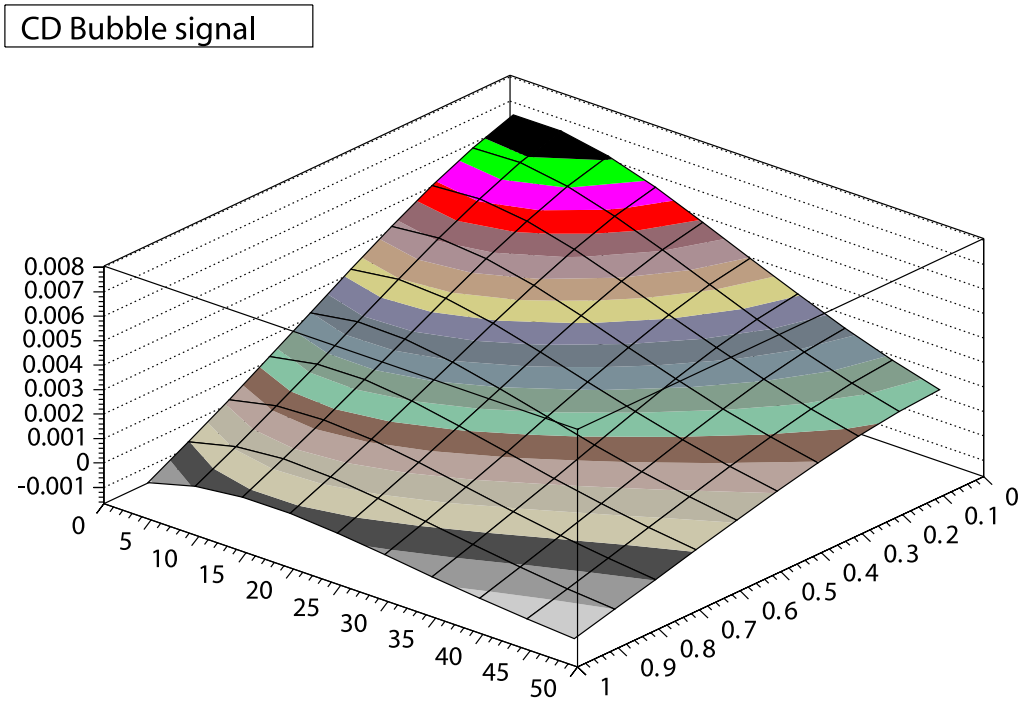

Fig. 9. A 2D perspective plot of $\Delta\Phi$ (*left side scale*) versus $\Delta\eta$ (*right side scale*) for the charge dependent correlation (CD) signal for track pairs from the same bubble. All other combinations of pairs are subtracted. This figure displays a measure of the 2D pair emission correlation of the unlike sign pairs of particles emitted from the same space-time region. The CD signal correlation is symmetric in $\Delta\Phi$ and $\Delta\eta$ ($\sim 30^\circ$ width in each)

which would correspond to an angle of 72°. Our bubbles are on the surface of the fireball when they emit individual particles and resonances which decay into particles. In the center of mass (CM) of the bubble which is moving with the surface half the particles are emitted outward from the surface. These are the ones which would be observed experimentally. Particles that are emitted from the interior region of the fireball have a large probability of being absorbed by the strongly interacting medium. These particles are also softer and are mainly below our p_t cut. The particles from the bubble that are emitted back toward the fireball would also be softer when their CM motion is subtracted from the motion in the rest frame of the bubble. Thus these particles also have a large probability of being absorbed by interaction with low momentum particles in the fireball or having their momentum reduced below our p_t cut. We will later on in Sect. 7 in this paper discuss all of the particles when comparing with data

that contain a large number of low energy particles, but generally we will only consider the particles above our p_t cut which are emitted on the outgoing surface of the bubble. Figure 7 shows the like-sign charged pair correlation signal coming from the same bubble. This figure is generally similar in appearance to the unlike-sign charged pairs except for a symmetric dip at small $\Delta\eta$ and $\Delta\Phi$ at $\Delta\eta$ centered near zero. This dip spreads about 15° in $\Delta\Phi$ and 0.3 in $\Delta\eta$ (which is approximately 15° in the η direction). In [1] we had determined that the $\Delta\Phi$ width of emission of a single particle was about 30°, and thus the expected $\Delta\Phi$ width for a particle pair would be approximately double, which is about 60°, in agreement with the $\Delta\Phi$ width of the unlike pairs signal and like pairs signal in Figs. 6 and 7.

When we were adjusting our bubble model to the RHIC data, we considered all charged pairs of tracks independent of their charge. This correlation is called the total charge independent (CI) correlation. The CI correlation is defined as the sum of the unlike-sign charged pairs total correlation and the like-sign charged pairs total correlation. The CI correlation is twice the correlation of all charged track pairs from a given bubble. Figure 8 shows the CI correlation signal for track pairs from the same bubble; all other combinations of track pairs are subtracted. The HIJING background does not contribute to these correlations as previously mentioned. Again the $\Delta\Phi$ range is from 0° to 180° and the $\Delta\eta$ is from 0.0 to 1.5. This figure displays the average correlation of particles coming from individual bubbles. The emission of particles from the bubble is by pair production from partons which are almost entirely gluons. The gluons produce colored pairs of quarks and antiquarks, which recombine into color singlets that have plus, zero, or minus charge. Thus a local neutral system contains charged particles, but the total charge has to add to zero. Particle production from a local phase space cell is what creates the dip in the small $\Delta\eta$ and $\Delta\Phi$ part of the like-sign charged pairs correlation in Fig. 7. Each local phase space cell has on the order of one color singlet pair. Since gluons emit unlike-sign charged pairs from the same phase space cell, like charged particle pairs emission from the same phase space region is suppressed.

If we subtract the like-sign charged pairs signal (Fig. 7) from the unlike-sign charged pairs signal (Fig. 6), we are left with the balancing plus and minus charge emissions which are emitted from the same space-time region. This correlation is called the charge dependent (CD) correlation

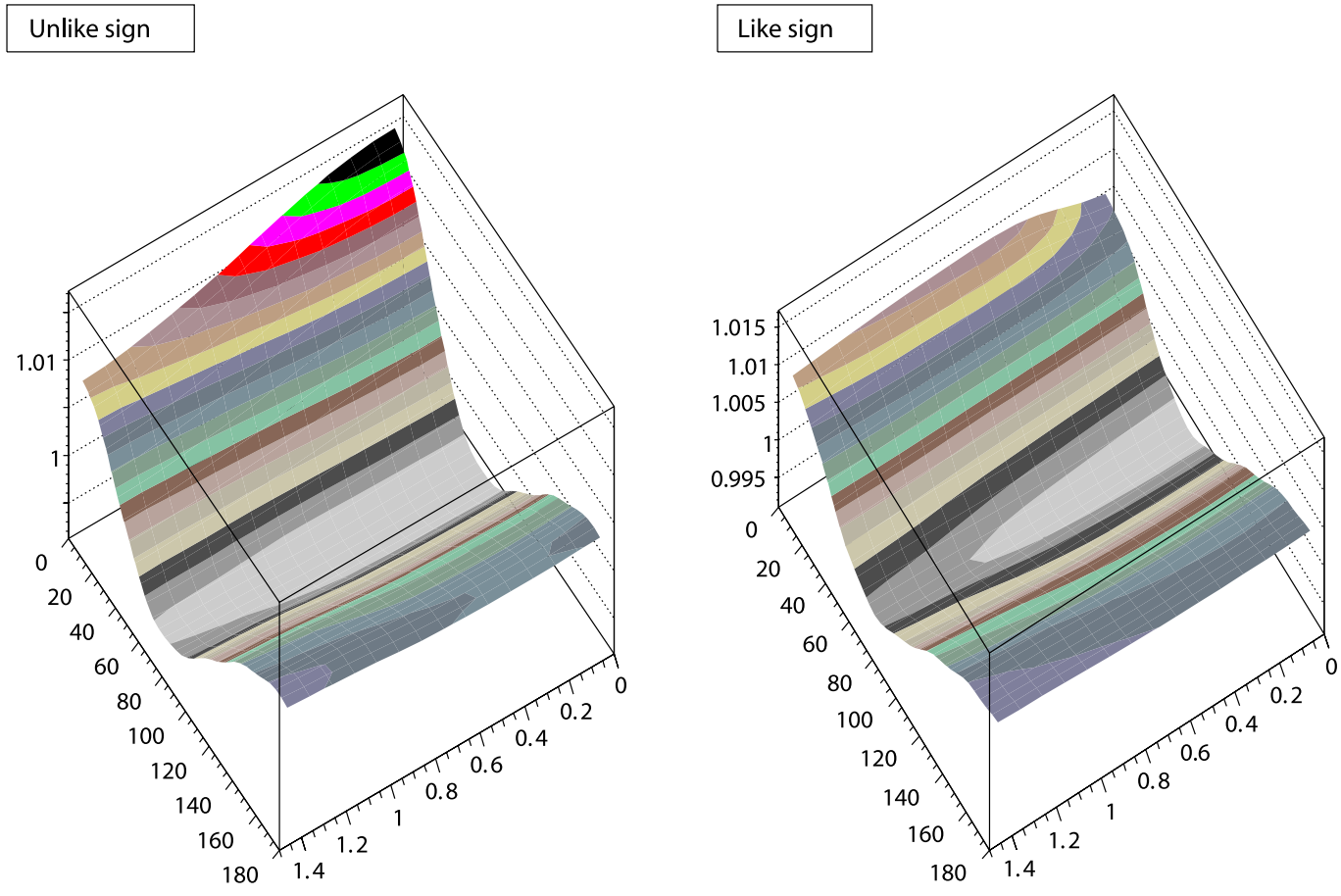

Fig. 10. The *left side* shows a 2D perspective plot of the total correlation (including background) for the unlike-sign charged pairs predicted by the parton bubble model. The *right side* shows the 2D total correlation (including background) for the like-sign charged pairs for the parton bubble model

signal. The CD correlation is defined as the subtraction of the like-sign charged pairs correlation from the unlike-sign charged pairs correlation, including background in each. This correlation, when observed experimentally, is within the errors the same as the CD signal which is defined as (the unlike charged pairs correlation minus the background) − (the like charged pairs correlation minus the background). This occurs since the backgrounds cancel in the subtraction.

A physical interpretation of the CD signal is that it displays a measure of the emission correlation of the opposite sign pairs of particles emitted from the same space-time region. The subtraction removes those pairs of opposite sign particles which do not come from the same space-time region. This CD signal correlation is shown in Fig. 9. In Fig. 9 the CD signal correlation is symmetric in the corresponding $\Delta\Phi$ and $\Delta\eta$ angular widths ($\sim 30°$). This is because the average pair has an opening angle between the plus and minus particle up to 60° in a random distribution about some fixed η and Φ direction for the bubble. There are some systematic errors in the fragmentation of the partons from the bubbles. To correct this we have kept the number of bubbles fixed and varied the fragmentation parameters, while keeping our agreement as good as seen in Figs. 3 and 4. In Table 1 we give the parameters of the bubble model only considering charged particles. The neutral particles are not included in the table.

4 Comparison of parton bubble model and high statistics STAR correlation experimental analysis

Reference [12] had a p_t cut of $0.8\,\mathrm{GeV}/c < p_t < 2.0\,\mathrm{GeV}/c$, consistent with our first multi-bubble model paper [1]. Therefore in making a comparison with this new STAR data analysis we have modified the parton bubble model to have the above p_t range. The STAR analysis of [25] used earlier was found to be consistent with the new analysis [12] for the CI $\Delta\Phi$ correlation in two $\Delta\eta$ bins. In the sections above we have treated the adjustment procedure used for the two variables of the model; which need to be determined are the longitudinal momenta of the partons and their number per bubble. The number of partons per bubble was 3–4 as determined previously.

4.1 Unlike-sign and like-sign charged pairs

There are two different basic types of pair correlations, unlike-sign charged pairs and like-sign charged pairs. Both experiment and theory contain signals and background correlations in these two pair types. The separation of signal and background is model dependent; thus we will compare the total experimentally observed correlation in STAR with the total correlation generated by

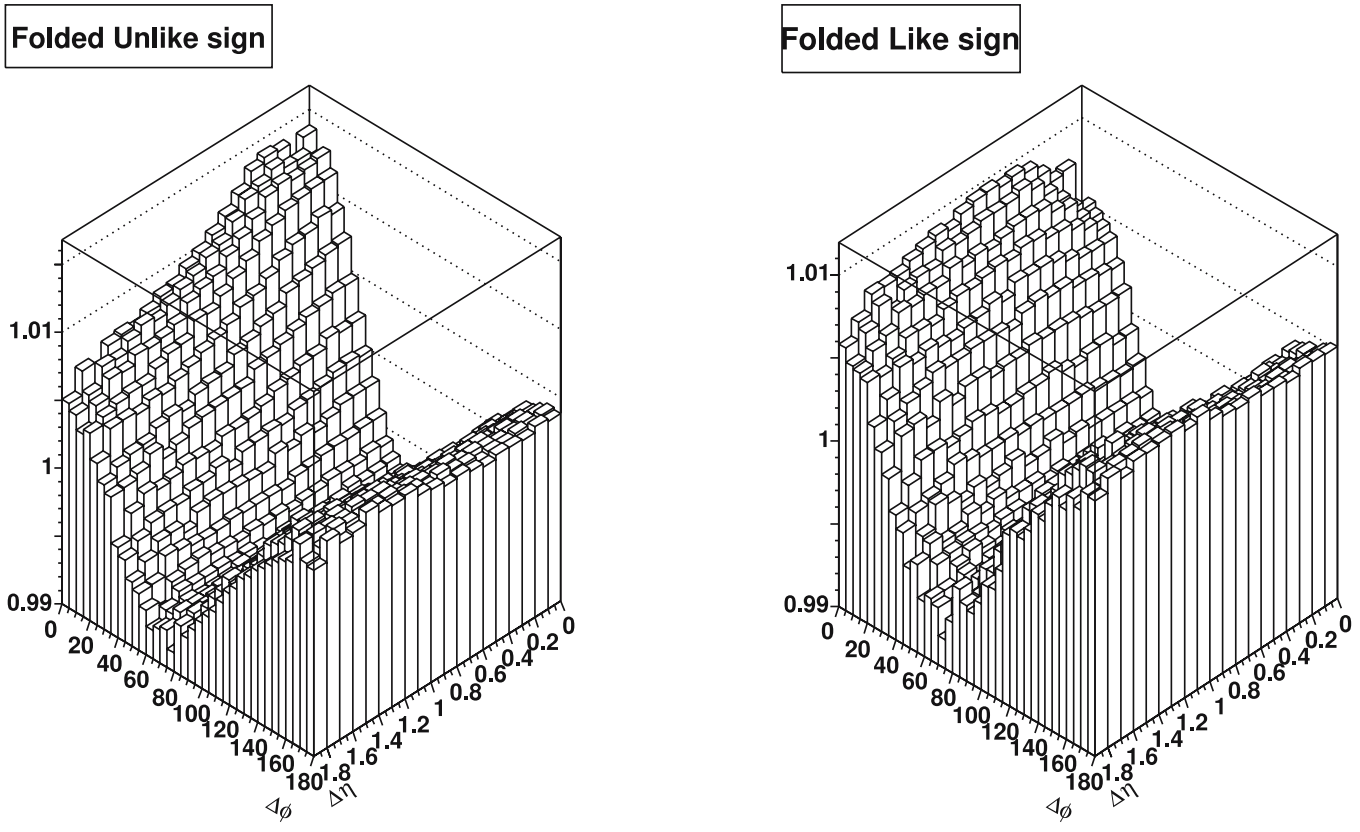

Fig. 11. The *left side* shows the 2D total correlation for the unlike-sign charged pairs determined in the STAR experiment. The *right side* shows the 2D total correlation for the like-sign charged pairs determined in the STAR experiment. When comparing Fig. 10 with Fig. 11 note the scale on the *right side* of Fig. 11 is somewhat enlarged compared to all other plots in Figs. 10 and 11

the parton bubble model. We have: total correlation = signal correlation + background correlation.

Figure 10, left side, shows a 2D perspective plot of the total correlation (including background) for the unlike-sign charged pairs predicted by the parton bubble model. The right side shows the 2D total correlation (including background) for the like-sign charged pairs for the parton bubble model.

Figure 11, left side, shows the 2D total correlation for the unlike-sign charged pairs determined in the STAR experiment. The right side shows the 2D total correlation for the like-sign charged pairs determined in the STAR experiment. When comparing, note that the scale on the right side of Fig. 11 is somewhat enlarged compared to all other plots in Figs. 10 and 11.

The parton bubble model predictions are in reasonable agreement with the experimental data. A quantitative comparison will be made for the important physically interpretable CI and CD total correlations in Sects. 4.2 and 4.3 respectively.

4.2 Charge independent correlation

The CI correlation is defined as CI = unlike-sign charge pairs correlation + like-sign charge pairs correlation. The CI correlation is the most important one, since it displays the average structure of the correlated emitting sources. As stated previously we need to compare the total experimental CI with the total parton bubble model CI. The analytic formulae for the experimental unlike-sign and like-sign charge pairs correlation are given in the STAR paper [12]. We generated two million 0–10% centrality events in order to compare with the CI correlation of STAR. In order to make a quantitative comparison we divide the 2D CI up into five $\Delta\eta$ bins as shown in Fig. 12. In each labeled $\Delta\eta$ bin we show the $\Delta\Phi$ total correlation for the CI as a function of $\Delta\Phi$. The STAR Au + Au central trigger analysis results from the formulae are shown as a solid line. The parton bubble model predictions are shown by the circular points, which are large enough to include the statistical errors from the 2 million events. In order to show all five $\Delta\eta$ bins, and the comparison between the model and the experiment, we use an offset technique. The vertical correlation scale is not offset for the largest $\Delta\eta$ bin, $1.2 < \Delta\eta < 1.5$, and is the lowest bin on the figure. As one proceeds upwards to the next bin $\Delta\eta$ the correlation is offset by +0.01. This is added to the correlation of each subsequent $\Delta\eta$ bin. The smallest $\Delta\eta$ on top of Fig. 12 has a +0.04 offset. A solid straight horizontal line shows the offset for each $\Delta\eta$ bin. Each solid straight horizontal line is at 1.0 in correlation strength.

The agreement between the parton bubble model and the STAR experimental analysis is very good in each of the five $\Delta\eta$ bins. The difference between the STAR experiment total CI and the parton bubble model predictions for them in the five $\Delta\eta$ bins considered are smaller than approximately 0.1%. This is 10% of the observed correlation. The average differences are smaller, namely, 4% for four of the $\Delta\eta$ bins and 5% for the smallest $\Delta\eta$ bin. Thus we have successfully explained the observed CI correlation in this high precision experimental analysis in a reasonably quantitative manner with the parton bubble model.

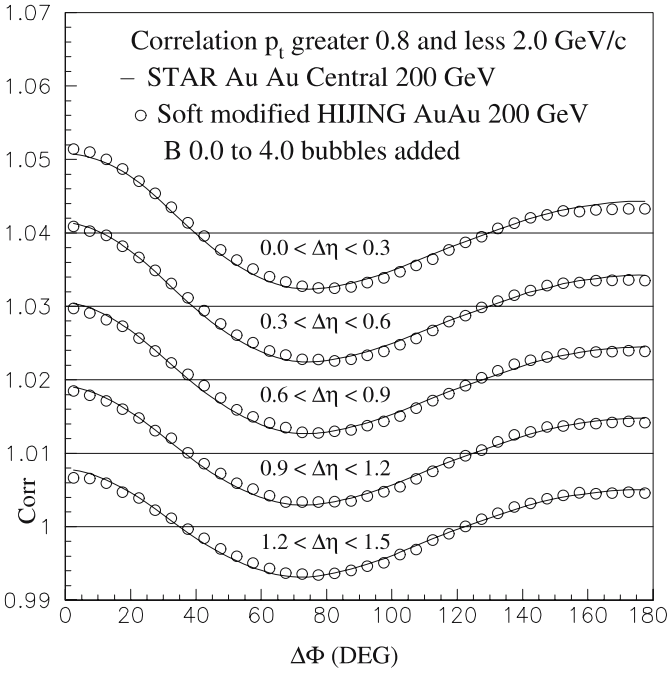

Fig. 12. In each of the five labeled $\Delta\eta$ bins we show the $\Delta\Phi$ total correlation for the CI as a function of $\Delta\Phi$. The STAR Au + Au central trigger analysis results from the formulae of [12] are shown as a *solid line*. The parton bubble model predictions are shown by the *circular points* (○) which are large enough to include the statistical errors from a 2 million event sample. The vertical correlation scale is not offset and is correct for the largest $\Delta\eta$ bin, $1.2 < \Delta\eta < 1.5$, and is the lowest bin on the figure. As one proceeds upwards to the next bin $\Delta\eta$ the correlation is offset by +0.01. This is added to the correlation of each subsequent $\Delta\eta$ bin. The smallest $\Delta\eta$ and *top* of Fig. 12 has a +0.04 offset. A *solid straight horizontal line* shows the offset for each $\Delta\eta$ bin. Each *solid straight horizontal line* is at 1.0 in correlation strength. The 0–10% centrality in HIJING corresponds to impact parameter (b) range 0.0 to 4.0 fm. The agreement is very good

4.3 Charge dependent correlation

The CD correlation is defined by CD = unlike-sign charge pairs correlation − like-sign charge pairs correlation. The subtraction of the like-sign charge pairs removes those pairs of unlike-sign particles that do not come from the same space-time region. Thus the CD is a measure of the correlation of the unlike-sign pairs which are emitted from the same space-time region. We are assuming in the model that the emission of particles almost entirely occurs from the bubbles on the surface of the fireball after freeze-out when there is no further interaction between particles. The bubbles are mainly made up of gluons and are almost neutral in charge.

Figure 13 shows a 2D perspective plot of the CD predicted by the parton bubble model. It displays the two

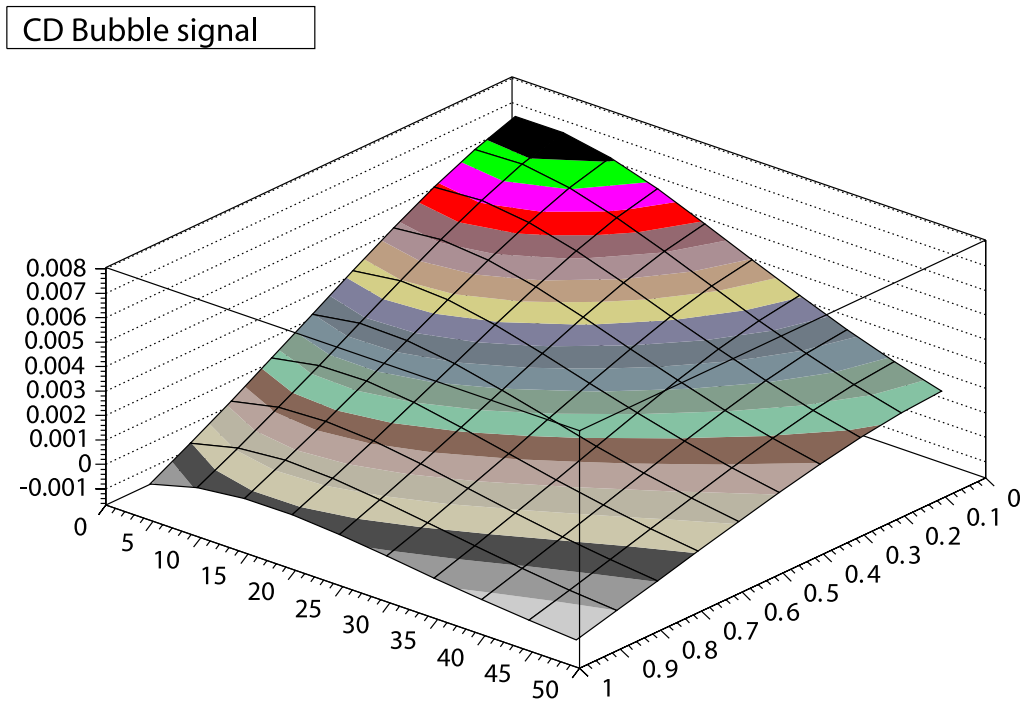

Fig. 13. A 2D perspective plot of the total CD correlation predicted by the parton bubble model. It is the same as the CD signal since the background cancels when one subtracts the like-sign charge pairs correlation from the unlike-sign charge pairs correlation. This correlation displays the unlike-sign charged pairs correlation from the same space-time region emitted from the surface of the fireball at freeze-out

dimensional correlation between unlike-sign charge pairs from the same space-time region emitted from the surface of the fireball at freeze-out. Figure 14 is the data plot in Fig. 6b from the STAR experimental paper [12] which is labeled as CD signal data. In the CD correlation the experimental backgrounds cancel almost entirely in the subtraction, so that the total CD is the same as the CD signal. In the parton bubble model they definitely cancel, so the total CD = the CD signal.

To quantitatively evaluate the agreement between the experimental CD and the parton bubble model CD, we make use of the relationship of the CD to the net charge fluctuation suppression. The net charge fluctuation suppression is directly related to an integral over the CD. We make a comparison of this suppression between the parton bubble model and the experimentally observed suppression. The net charge fluctuation suppression is the observed percentage reduction in the RMS width of the distribution of the event by event difference of the number of positive tracks minus the negative tracks, compared to the RMS width of a random distribution.

We performed a charge difference analysis for the parton bubble model particles within the same cuts as the STAR experimental paper [12], which were $0.8 < p_t < 2.0\,\mathrm{GeV}/c$ and $|\eta| < 0.75$, and used the same method described there. For each parton bubble model event we determined the difference of the positive particles minus the negative particles in our cuts. There was for the sum of these a net mean positive charge of 4.70 ± 0.01. The width of the charge difference distribution was given by the RMS as 10.82 ± 0.01. To determine the net charge fluctuation suppression we need to compare this width with the width of the same set of particles with a random charge assigned. Then this distribution would have no net charge fluctuation suppression.

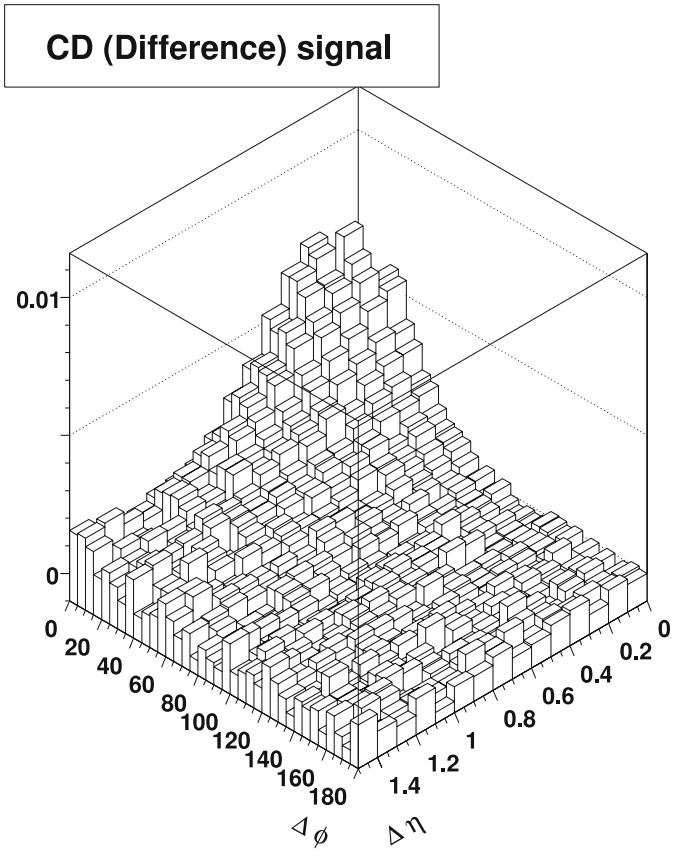

Fig. 14. The CD signal determined by the STAR experimental analysis. It is observed to be the same as the total CD correlation. In Sect. 4.3 it is shown via a quantitative analysis that in Fig. 14 the experiment agrees in the integral with Fig. 13 the parton bubble model

However, we must arrange a slight bias toward a positive charge particle so that we will end up with the same net mean positive charge. We now cycle through the events assigning a random charge to each particle with a slight bias toward being positive, we obtain a mean of 4.70 ± 0.01 and width (RMS) of 11.47 ± 0.01. The percentage difference in the width which measures the net charge fluctuation suppression is $5.7\% \pm 0.2\%$. The results of the experimental STAR analysis [12] were that the net charge fluctuation suppression value was $6.0\% \pm 0.2\%$, and the mean net charge was 4.68 ± 0.01. The parton bubble model results agree within the errors with the STAR experimental analysis results. Thus the CD for both agree quantitatively.

Thus we have demonstrated that the parton bubble model can quantitatively explain the total CI and the total CD experimentally determined correlations [12]. Since the unlike-sign and like-sign total correlation are linear combinations of the CI and CD, it is implied that they are also quantitatively explained. Hence all total correlations in this high statistics experimental analysis, with well understood systematics, are quantitatively in agreement with the parton bubble model.

5 Quark–quark recombination

We have shown previously that inside the bubble there are 3–4 partons with differing longitudinal momenta all at the same Φ. The p_t distribution of the partons inside the bubble is similar to pQCD but has a suppression in the high p_t region like the data [16, 17]. The showering of the partons form gluons which fragment into quarks and antiquarks which overlap with each other in space and time. This leads to and enhances the possibility that pairs of quarks from two different fragmenting partons can form a di-quark, since the recombining partons are localized together in a small volume. The same process will happen for pairs of antiquarks forming a di-antiquark. This recombination process becomes an important possibility in our parton bubble model compared to regular jet fragmentation. Since the quarks which overlap have similar phase space, the momentum of the di-quark is approximately twice the momentum of the quarks but has approximately the same velocity. When mesons are formed quarks pick up antiquarks with similar phase space from fragmenting gluons to form a color singlet state. Thus the meson has approximately twice the momentum of the quark and antiquark of which it is made. When the di-quark picks up a quark and forms a color singlet it will have approximately 3 times the momentum of one of the three quarks it is made from. Thus we expect p_t spectrum scaling when we compare mesons to baryons. Figure 15 shows the ratio of protons plus antiprotons to charged particles as a function of p_t for particles in our simulated central Au + Au collisions. In Fig. 15 we also plot the ratio from central Au + Au RHIC data [26]. These experimental results agree well (considering the errors) with the bubble model predictions for all charged particles. The background particles from HIJING have the same ratios observed in *pp* colli-

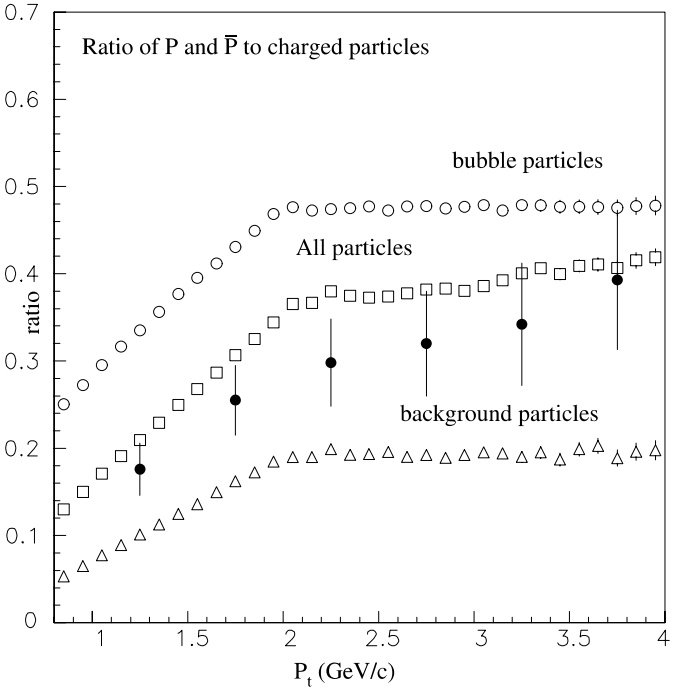

Fig. 15. Shows the ratio of protons plus antiprotons to charged particles as a function of p_t for particles in our simulated central Au + Au collisions. We also plot the ratio from central Au + Au RHIC data [26]. These experimental results agree well (considering the errors) with the bubble model predictions for all charged particles. The plotted ratio for the background particles in HIJING is similar to *pp* collisions

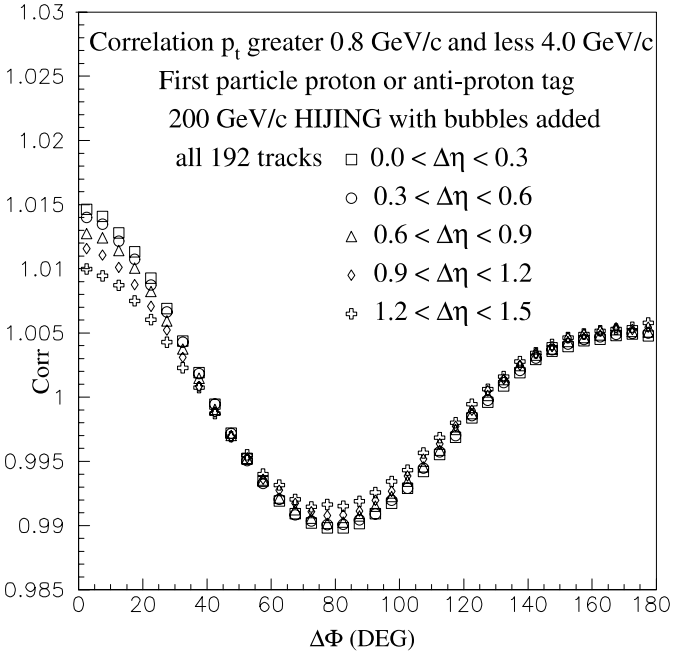

Fig. 16. Predicted correlation for $\Delta\Phi$ in the $0.0 < \Delta\eta < 0.3$ bin, $0.3 < \Delta\eta < 0.6$, $0.6 < \Delta\eta < 0.9$, $0.9 < \Delta\eta < 1.2$, and $1.2 < \Delta\eta < 1.5$ bins, when the first particle is tagged as a proton or antiproton

sions, while particles coming from our bubbles have a much larger ratio.

Recombination is an important aspect of our bubble model and leads to a prediction for the proton and antiproton tagged spectrum for example. We form $\Delta\Phi$ correlations for our usual five $\Delta\eta$ bins using a proton or antiproton tagged as our reference. The $\Delta\Phi$ is measured from the tagged proton or antiproton to another charged particle (this particle can also be a proton or antiproton). The $\Delta\Phi$ is folded to lie between 0° to 180°. The $\delta\eta$ is done in the same way and is folded about $\Delta\eta$ equal zero. Figure 16 shows the $\Delta\Phi$ correlation for our five standard $\Delta\eta$ bins (0.0 to 0.3, 0.3 to 0.6, 0.6 to 0.9, 0.9 to 1.2 and 1.2 to 1.5). By comparison we find that we predict that this correlation is only slightly stronger than our CI correlation for all charged particles. Of course correlations of other two-particle combinations can be predicted by the model and compared to available data and other model predictions.

6 Parton bubble model compared to standard HIJING

In this section we make a comparison with standard HIJING [20] with jet quenching turned off. With quenching off HIJING gives an inclusive p_{t} spectrum of charged particles above 3.0 GeV/c which is consistent with binary scaling of [16, 17]. In [1] we found that the expected QCD jets from HIJING at $\sqrt{s_{NN}} = 130$ GeV for 0–10% centrality Au + Au led to a scale factor which was about half that from the bubble model. This was confirmed when we doubled the number of jets in HIJING. However the width of jets in $\Delta\eta$ is much narrower for HIJING (or QCD jets) than for bubbles. In [25] we showed a comparison of STAR $\sqrt{s_{NN}} = 200$ GeV correlation data for 0–10% centrality Au + Au with HIJING that also had twice the jets added. From this reference we compared the $\Delta\Phi$ correlation for two $\Delta\eta$ bins 0.0 to 0.3 and 0.6 to 0.9. Again the width in $\Delta\eta$ of the jets was much less compared to the data that we adjusted our bubble model to.

In this section we have chosen to make a comparison of our bubble model with the standard HIJING (with no jet quenching) for all of our $\Delta\eta$ bins and for the two-particle CI $\Delta\Phi$ correlations. Figure 17 shows the two-particle CI $\Delta\Phi$ correlation for our five standard $\Delta\eta$ bins (0.0 to 0.3, 0.3 to 0.6, 0.6 to 0.9, 0.9 to 1.2 and 1.2 to 1.5). We used the same offset technique on the correlation scale as for Fig. 12. The vertical correlation scale is not offset for the largest $\Delta\eta$ bin, $1.2 < \Delta\eta < 1.5$, and it is the lowest bin on the figure. As one proceeds upwards to the next bin $\Delta\eta$ the correlation is offset by +0.01. This is added to the correlation of each subsequent $\Delta\eta$ bin. For the smallest $\Delta\eta$ the top of Fig. 12 has a +0.04 offset. A solid straight horizontal line shows the offset for each $\Delta\eta$ bin. Each solid straight horizontal line is at 1.0 in correlation strength. The HIJING results differ greatly from the bubble model predictions.

Let us compare the HIJING jet properties (Table 2) to our bubble model. We have only 12 bubbles compared to the 26 jets of HIJING which is a mere factor of 2.

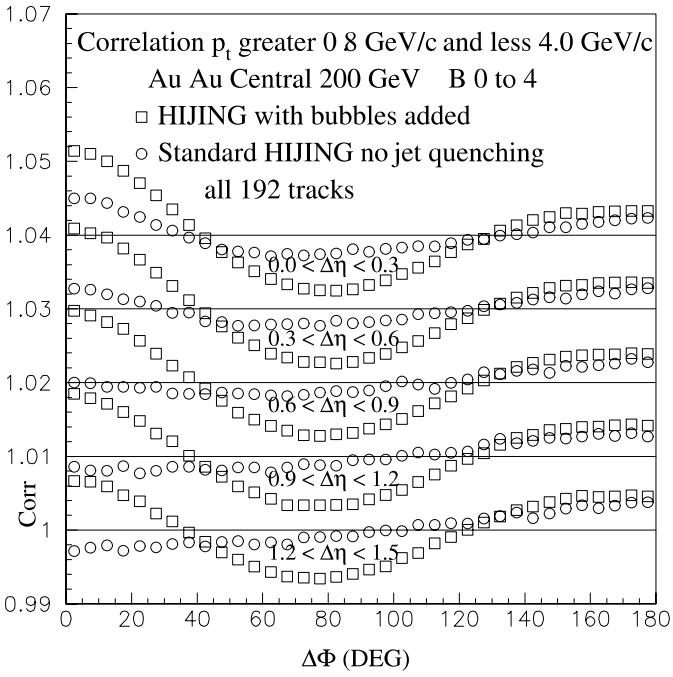

Fig. 17. The bubble model two particle CI correlation compared to standard HIJING (without quenching) CI. In each of the five labeled $\Delta\eta$ bins we show the $\Delta\Phi$ total correlation for the CI as a function of $\Delta\Phi$. The *vertical correlation scale* is not offset and is correct for the largest $\Delta\eta$ bin, $1.2 < \Delta\eta < 1.5$, and is the lowest bin on the figure. As one proceeds upwards to the next bin $\Delta\eta$, the correlation is offset by +0.01. This is added to the correlation of each subsequent $\Delta\eta$ bin. The smallest $\Delta\eta$ and top of Fig. 17 has a +0.04 offset. A *solid straight horizontal line* shows the offset for each $\Delta\eta$ bin. Each *solid straight horizontal line* is at 1.0 in correlation strength. The 0–10% centrality in HIJING corresponds to impact parameter (b) range 0.0 to 4.0 fm

Each jet on the average has three charged particles compared to seven from a bubble, another factor 2. Thus the number of charged particles from correlated objects is about the same, 78 compared to 88. However, the bubble model (modified HIJING with bubbles replacing the jets) in Fig. 17 has a much larger correlation, near $\Delta\Phi$ and $\Delta\eta$ equal 0, and it has a much larger $\Delta\eta$ width than the jets. The above facts are understood when we consider that the total energy in charged particles from jets is 57 GeV and is 116 GeV for bubbles (more than twice as much). Since the charged particles that fragment from jets are close to the

Table 2. Parameters of HIJING jets for charged particles

Variable	Amount
Jets	26
Particles	3
Soft	114
p_{t} (GeV/c)	2.2
Energy (GeV)	2.2

same η (modest spread in $\Delta\eta$) the energy per jet is approximately the same as the sum p_t per jet.

7 Soft particles from bubbles on the surface

We have chosen our p_t range in order to resolve the individual bubbles on the surface of the expanding fireball of the Au + Au collision. We have assumed that particles from a lower p_t range mainly come from inside the fireball since the HBT radii of soft pions is around 6 fm. However there are charged particles that would come from the bubble which are below the 0.8 GeV/c p_t cut which was imposed. Many of these particles could be mixed in with the soft particles from the fireball and could easily undergo re-scattering with the soft particles and lose their correlation with each other and with particles which are above 0.8 GeV/c. On the average each bubble creates 45 charged particles, where only seven are above 0.8 GeV/c. The average sum p_t of the bubble is 11 GeV/c with 6 GeV/c or 58% coming from the seven particles above 0.8 GeV/c. The total rest frame energy from the 45 charged particles is 27 GeV which is 3 times the 9 GeV that goes into the seven particles above 0.8 GeV/c. Thus above our p_t cut we detect 58% of the momentum and 33% of the energy of the bubble.

Reference [27] has fitted Au + Au CI $\Delta\Phi$ versus $\Delta\eta$ correlations for a p_t range 0.15 to 2.0 GeV/c. It is possible to compare these results with our bubble model under the assumption that none of our soft charged particles interact in the final state. We believe that this would be highly unlikely and such a comparison would be an upper limit to the correlation from the lower p_t particles. If the observed correlation is larger than our upper limit, then there must be more sources of correlated particles. In this comparison we are not considering the possibility that bubbles which exist inside the fireball may also contribute some angular correlations. We are only considering surface bubbles which emit charged particles after freeze-out and that do not interact in the final state. The 45 charged particles per bubble times 12 bubbles approximately equals 540 particles that are added to the soft particles from the HIJING beam jets. If we use the p_t range of [27], we obtain 535 charged particles from bubbles resulting in, on the average, 1135 charged particles per event when the soft particles of the beam jets are added. Figure 18 shows the two-particle CI $\Delta\Phi$ correlation for our five standard $\Delta\eta$ bins (0.0 to 0.3, 0.3 to 0.6, 0.6 to 0.9, 0.9 to 1.2 and 1.2 to 1.5). We used the same offset technique on the correlation scale as for Fig. 12. The vertical correlation scale is not offset for the largest $\Delta\eta$ bin, $1.2 < \Delta\eta < 1.5$, and it is the lowest bin on the figure. As one proceeds upwards to the next bin $\Delta\eta$, the correlation is offset by +0.01. This is added to the correlation of each subsequent $\Delta\eta$ bin. For the smallest $\Delta\eta$ the top of Fig. 12 has a +0.04 offset. A solid straight horizontal line shows the offset for each $\Delta\eta$ bin. Each solid straight horizontal line is at 1.0 in correlation strength. The curves are from [27] where the fits were done on mid-rapidity Au + Au central events at $\sqrt{s_{NN}} = 130$ GeV. Here we have compared the results of our bubble model with the experimental $\sqrt{s_{NN}} = 130$ GeV correlation which does not change a lot from $\sqrt{s_{NN}} = 200$ GeV to 130 GeV. From our analyses we conclude that the parton bubble model predictions with the number of hot spots (bubbles) and their content are relatively insensitive to a decrease of $\sqrt{s_{NN}} = 200$ GeV to 130 GeV. We attribute the difference in the correlation of Fig. 18 to re-scattering of the low p_t particles and they are not significantly due to the energy difference. Using our regular p_t cuts we avoid the re-scattering problem of the soft particles.

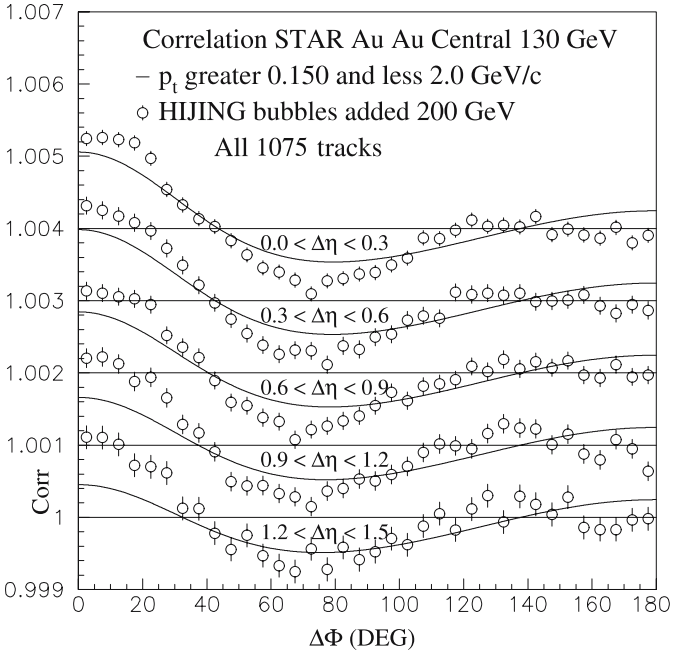

Fig. 18. Comparison of the CI correlation of the bubble model prediction for $\sqrt{s_{NN}} = 200$ GeV with experimental results at $\sqrt{s_{NN}} = 130$ GeV. In each of the five labeled $\Delta\eta$ bins we show the $\Delta\Phi$ total correlation for the CI as a function of $\Delta\Phi$. The vertical correlation scale is not offset and is correct for the largest $\Delta\eta$ bin, $1.2 < \Delta\eta < 1.5$, and is the lowest bin on the figure. As one proceeds upwards to the next $\Delta\eta$ bin, the correlation is offset by +0.01. This is added to the correlation of each subsequent $\Delta\eta$ bin. The smallest $\Delta\eta$ and *top* of Fig. 18 has a +0.04 offset. A *solid straight horizontal line* shows the offset for each $\Delta\eta$ bin. Each *solid straight horizontal line* is at 1.0 in correlation strength. See Sect. 7 of the text for approximations made and discussion

Note the qualitative similarity of the bubble model predictions and the correlation data fit it is compared with. Generally the correlation of the data as a function of $\Delta\Phi$ is smaller for each $\Delta\eta$ bin particularly in the near forward angles where the bubble model contribution is largest. The above study seems to be consistent with surface emission from bubbles as expected from the bubble model with roughly half of the charged particles at the lower p_t being rescattered as they make their way out of the interior of the fireball. These ideas are consistent with jet quenching of [16, 17] and large energy loss if any parton tries to move across the interior region of the fireball. Thus the large angular correlations that are seen at RHIC [27] are explained

as due to bubble hot spots on the surface of the fireball at freeze-out.

8 Summary and discussion

In this article we revisit our bubble model [1]. We expanded the model to successfully reach our goal of developing a parton inspired model for these bubbles and describe how the bubble of partons fragments into charged particles. With the help of RHIC data [25] we were able to adjust the model and determine the number of partons (3–4 essentially all gluons) in a bubble and their longitudinal momenta at a fixed Φ. Experimental information [16, 17] about how strong jet quenching is allowed us to expand the upper limit of transverse momentum (p_t) to 4.0 GeV/c, which includes the quark–quark recombination region without including a significant jet contamination. Our earlier paper [1] chose to avoid the p_t range above 2.0 GeV/c in order to exclude significant jet effects. Utilizing more recently available data we have been able to make the approximation for central Au + Au collisions that jets play a small part in our increased $0.8\,\mathrm{GeV}/c < p_t < 4.0\,\mathrm{GeV}/c$ range, unless one triggers on high p_t particles. Thus for our un-triggered particle correlations in the bubble model, jets can be ignored. In the longitudinal phase space of our fragmenting bubbles quark–quark recombination gives the same velocity to di-quarks and thus twice the transverse momentum. This recombination increases the number of baryons and antibaryons in the parton fragmentation of the bubble compared to the normal yield of jet fragmentation. In Fig. 15 we show experimental data which agree with the bubble model prediction of the ratio of proton plus antiproton to all charged particles as a function of p_t (see Sect. 5).

In Sect. 7 and Fig. 18, we compared the predictions of the bubble model with the correlation data analysis of $\Delta\Phi$–$\Delta\eta$ in [27]. This experiment observed particles in the p_t range of 0.15 to 2.0 GeV/c. Thus most of the particles had a lower p_t than the cut $> 0.8\,\mathrm{GeV}/c$ that we normally use in the bubble model. However, we were able to show that the $\Delta\Phi$–$\Delta\eta$ correlations observed were in qualitative agreement with the emission of particles from the fireball surface bubbles as predicted by the bubble model.

We have made many quantitative predictions for two-particle correlations that can be quantitatively tested by high precision data from RHIC. The predictions in this paper are only a fraction of what the parton bubble model can generate quantitatively as needed to compare with the correlation data of interest as they become available.

We will below in this section summarize a quantitative successful comparison with a high statistics STAR experimental analysis [12] described in Sect. 4.

The geometry of the expanding fireball surface along with the HBT source size of about 2 fm radius chosen for our adjoining bubbles lead to 12 bubbles in an 8 fm radius ring, perpendicular to and centered around the beam. The bubble ring is wrapped around the outer surface of the fireball at mid-rapidity [1]. We have seen from Table 1 that each bubble on the average has a p_t value of 6 GeV/c when we consider charged particles above 0.8 GeV/c. We also found that when we consider soft particles from the bubble the charged particles account for a p_t of 11 GeV/c. If we now consider the neutral contribution, we end up with p_t around 16 GeV/c per bubble. We have shown in Sect. 7 that each bubble on the average contains 27 GeV of energy in charged particles which increases to 40 GeV when we consider the neutral particles. It is of interest to note that on the average each bubble contains approximately one-thousandth of the total initial energy of the Au + Au system. Since we have 12 bubbles, this implies that there is 480 GeV or ~ 500 GeV of energy stored in the bubbles on the surface of the fireball in the mid-rapidity region.

In Sect. 6 we compare the standard HIJING with the parton bubble model and found that they differ greatly (see Fig. 17).

Here we summarize a comparison of the parton bubble model predictions with a recent high statistics STAR two-particle correlation paper [12]. This paper has systematic errors that are well understood and have no significant effects on its conclusions.

We have modified the p_t and η cuts in the parton bubble model in order to correspond to the cuts in the analyses of the high precision STAR experiment [12] for central Au + Au $\Delta\Phi$–$\Delta\eta$ correlations at $\sqrt{s_{NN}} = 200$ GeV. We have shown that the bubble model predictions agree reasonably quantitatively with the experimental analyses of the total CI and total CD correlations.

The CI correlation displays the average structure of the correlated emitting sources. The differences between the STAR experiment's total CI correlation and the parton bubble model's total CI predictions for the five $\Delta\eta$ bins compared are smaller than $\sim 0.1\%$. This is 10% of the observed correlation. The average differences are even smaller, namely, 4% for four of the $\Delta\eta$ bins and 5% for the first and smallest $\Delta\eta$ bin.

The quantitative comparison of the total CD correlation of the STAR experiment and the parton bubble model was made by comparing the net fluctuation suppression which is related to the integral of the total CD. The net charge fluctuation suppression was $6.0\% \pm 0.2\%$ for the STAR experiment and $5.7\% \pm 0.2\%$ for the parton bubble model. The net mean positive charge for the experiment was 4.68 ± 0.01 and 4.70 ± 0.01 for the parton bubble model. These values agree within errors.

Thus we observed good quantitative agreements with a high precision correlation analysis which was performed under conditions closely to those incorporated in the parton bubble model. This implies substantial evidence for the basic properties of the parton bubble model being consistent with the dominant characteristics present in the data.

These observed characteristics of the parton bubble model, which lead to the good quantitative agreement of the CI and CD correlation, imply that the individual sources of correlated particles are consistent with localized gluonic hot spots which reside on the surface of the fireball.

Our first goal is to establish the existence of a bubble type substructure after successful comparison with other

relevant high precision data which become available. Our ultimate goal is to investigate the nature and content of the bubble structure and determine if it has final state properties implying a QGP.

Acknowledgements. The authors thank William Love for valuable discussions and assistance in production of the figures.

This research was supported by the U.S. Department of Energy under Contract No. DE-AC02-98CH10886 and the City College of New York Physics Department

References

1. S.J. Lindenbaum, R.S. Longacre, M. Kramer, Eur. Phys. J. C **30**, 241 (2003)
2. L. van Hove, Z. Phys. C **27**, 135 (1985)
3. L. Schroeder, S.J. Lindenbaum, Proc. RHIC Workshop: Experiments for Relativistic Heavy Ion Collider, April 15–19, 1985, ed. by P.E. Haustein, C.L. Woody (Brookhaven National Laboratory, Upton, New York), pp. 211–252
4. S.J. Lindenbaum, Proc. Second Workshop on Experiments and Detectors for Relativistic Heavy Ion Collider (RHIC), May 25–29, 1987, ed. by H.G. Ritter, A. Shor (Lawrence Berkeley Laboratory, Berkeley, California), pp. 146–165
5. S.J. Lindenbaum, Proc. Third Workshop on Experiments and Detectors for Relativistic Heavy Ion Collider (RHIC), Brookhaven National Laboratory, July 11–22, 1988, ed. by B. Sivakumar, P. Vincent (Brookhaven National Laboratory, Upton, New York), pp. 82–96
6. S.J. Lindenbaum et al., Proc. Fourth Workshop on Experiments and Detectors for Relativistic Heavy Ion Collider (RHIC), Brookhaven National Laboratory, July 2–7, 1990, ed. by M. Fatyga, B. Moskowitz (Brookhaven National Laboratory, Upton, New York), pp. 169–206
7. S.J. Lindenbaum, R.S. Longacre, J. Phys. G **26**, 937 (2000)
8. J. Adams et al., Phys. Rev. C **70**, 054907 (2004)
9. F. Karsch, Nucl. Phys. A **698**, 199 (2002)
10. J. Adams et al., Phys. Rev. C **71**, 044906 (2005)
11. S.S. Adler et al., Phys. Rev. Lett. **93**, 152302 (2004)
12. STAR Collaboration, J. Adams et al., nucl-ex/0607003, submitted to Phys. Rev. C
13. A. Dumitru, R.D. Pisarski, Phys. Lett. B **504**, 282 (2001)
14. M. Gyulassy, D. Rischke, B. Zhang, Nucl. Phys. A **613**, 397 (1997)
15. H.J. Drescher et al., Phys. Rev. C **65**, 054902 (2002)
16. C. Adler et al., Phys. Rev. Lett. **87**, 112303 (2001)
17. C. Adler et al., Phys. Rev. Lett. **92**, 112301 (2004)
18. J. Adams et al., Phys. Rev. Lett. **95**, 152301 (2005)
19. R.J. Fries, B. Muller, C. Nonaka, S.A. Bass, Phys. Rev. C **68**, 044902 (2003)
20. X.N. Wang, M. Gyulassy, Phys. Rev. D **44**, 3501 (1991)
21. K.H. Ackerman et al., Phys. Rev. Lett. **86**, 402 (2001)
22. C. Adler et al., Phys. Rev. Lett. **90**, 032301 (2003)
23. J. Adams et al., Phys. Rev. C **72**, 014904 (2005)
24. T. Sjostrand, M. van Zijil, Phys. Rev. D **36**, 2019 (1987)
25. STAR Collaboration, R.S. Longacre, Proc. International Workshop on Light Cone Physics: Hadron and Beyond, Institute for Particle Physics Phenomenology, University of Durham, UK, Aug. 5–9, 2003, ed. by S. Dalley, pp. 110–117
26. S.S. Adler et al., Phys. Rev. Lett. **91**, 172301 (2003)
27. J. Adams et al., Phys. Rev. C **73**, 064907 (2006)